university of groningen

Faculty of Science and Engineering

Bachelor Thesis

Modeling quantum diffusion in linear aggregates coupled to colored noise baths

Author:
Hans Douwe Wobben
S2775484

Supervisor:
Prof. dr. T.L.C. Jansen
Prof. dr. A. Borschevsky

A thesis submitted in fulfillment of the requirements for the degree of Bachelor of Science

July 1, 2022

Abstract

During photosynthesis, photon energy is absorbed by chromophore molecules, causing electronic excitations. The excitation energy is then transported across molecules to the reaction center. Photosynthetic organisms accomplish this extremely efficiently, exceeding 90%. The prospect of better solar cell efficiency has driven the development of artificial light-harvesting systems. The excitation energy transport (EET) is quantum mechanical in nature and arises from the complex interplay of the chromophores and their environment. Current theories can explain EET in the weak and strong system-environment coupling regimes quite well, however in the intermediate regime the EET is much less understood. This research investigates the effect of white and colored noise environments on the excitation diffusion by simulating linear 1D aggregates using the white noise Haken-Strobl-Reineker (HSR) model and the colored noise Numerical integration of the Schrödinger equation (NISE) model. While the two models produce similar results in some parameter regimes, in general the difference is significant. Due to the colored noise, the NISE model has an extra parameter that causes rich behavior compared to the HSR model. The results therefore show that the addition of colored noise is crucial. Thus, even though NISE method is computationally more expensive than the HSR model it is worth investigating further.

Contents

Chapter 1

Introduction

Charge- or energy transfer in or across materials is an important topic in modern material science. A full understanding of the matter requires a multidisciplinary approach, combining chemistry, atomic and molecular physics, quantum mechanics, statistical mechanics, and thermodynamics. This research will focus on the quantum mechanical description of energy transfer as a result of the diffusion of excited energy states across a material. In particular, I will model the excitation energy diffusion in three different ways and compare them.

In order for a system to exhibit this kind of diffusion, there must be multiple coupled 'sites' present that are physically separated, between which excitation energy can be transferred. This configuration can be found in a range of systems, for example in large complex molecules or in chains of molecules. These systems can be found in nature and have also been created synthetically.

In nature, excitation energy transfer (EET) plays a crucial role in the photosynthesis process. During photosynthesis, chromophore molecules absorb light, causing excitations that are then transported across molecules towards a reaction center. Take, for instance, the PC 645 chromophore found in cryptophyte algae. The excitation transfer dynamics of PC 645 have been studied using a model containing 8 sites [1–4]. Other well known examples are the bacterial complexes LH1 [5] and LH2 [6].

By taking inspiration from nature, artificial light harvesting systems have been synthesized in the lab. These materials can be used for a wide range of applications, such as organic solar cells [7]. An example of synthetic light harvesting systems are C8S3-based nanotubes which have been studied extensively [8–10] and have been used to probe the relation between structural hierarchy and exciton diffusion [11]. A better understanding of exciton diffusion will allow us to construct more efficient light harvesting systems.

To improve our understanding of the EET process, experiments have measured optical properties of polymer aggregates. The experiments include single-molecule spectroscopy, coherent two-dimensional (2D) spectroscopy, and single-molecule coherent spectroscopy [7]. It is very hard to measure the diffusion directly due to the short energy transfer time scales ($\leq$ 1 ps) and the short diffusion lengths ($\leq$ 100 nm) involved, requiring simultaneous high spacial and temporal resolution. However, ultrafast transient absorption microscopy has been used to directly image exciton transport in synthetic meso-tetra(4-sulfona- tophenyl) porphyrin (TPPS4) molecules [12]. These experiments are important since they give information about the relevant electronic states that play a role in the diffusion. This information is used to verify and improve the theoretical models.

There are various approaches to modeling the diffusion. In every model, the system is coupled to a heat bath environment and the interaction between these two is what causes the EET behavior. Most methods involve simplifying assumptions and approximations to cut down on computation time at the cost of reduced accuracy

in the regimes where the approximations are not valid. There are too many models to mention here, so I will name only some prominent and relevant ones. The most important model is the Hierarchical Equations of Motion (HEOM) model. While it is very computationally expensive, it is also the most general method and, more importantly, numerically exact [13]. It scales poorly to large systems, but for small systems it is the 'gold standard' against which other methods can be compared. Another well known model is Redfield theory [14], which can model the population dynamics when the system is weakly coupled to a white noise bath. Then there is the Numerical integration of the Schrödinger equation (NISE) method, a very simple yet effective method which propagates the wave function to simulate the evolution of an exciton. NISE is not limited to white noise and scales reasonably well, but it is only valid in the high temperature limit. Finally, there is the Haken-Strobl-Reineker (HSR) model [15], which solves a stochastic Schrödinger equation for white noise heat baths. The HSR model is simple and scales excellently with system size.

The goal of this thesis is to investigate the effect of colored noise on diffusion. For simplicity, a linear 1D chain will be used as a model system. Both the HSR model and NISE model are simple to implement and they will be used in this research. The HSR model has excellent scaling, but is limited to white noise. While NISE does not have this limitation, its scaling is worse. To find a middle ground, the idea is to remove the white noise approximation from the HSR model and combine this with NISE. This should yield a more realistic model at the expense of computation time. The models will be compared over a range of parameters. Properties like accuracy and convergence rate will be of particular interest to evaluate the feasibility of the new method. The central research question of this thesis therefore

What effect does colored noise have on electronic energy diffusion and how do the models used to simulate this compare?

Chapter 2

Methods

2.1 System and model

2.1.1 Aggregate description

The system investigated in this thesis is a general linear 1D aggregate. The aggregate contains a number of coupled sites that can be described as two-level systems each with an electronic ground state and an excited state. In practice, the aggregate can be anything from a single chromophore molecule containing a number of sites to a polymer where each sub unit has one site [16, 17].

When an electron gets excited at one of the sites a "hole" is left behind in the ground state and the electron now occupies the excited state. The result is an exciton. Because of the coupling between sites, the electron and hole can move around on the aggregate. I will focus on the case where the electron and hole are on the same site, i.e. Frenkel excitons. This assumption is accurate when the overlap of the electronic charge densities of neighboring sites is sufficiently small [18]. This is often the case for organic molecules of interest [19].

The coupling between sites arises from quantum mechanical transition dipole interactions. The Hamiltonian term for the interaction between two dipoles is given as [20]

$$\hat{J}_{\text{dip}} = \frac{1}{4\pi\epsilon_0}\left(\frac{\hat{\boldsymbol{\mu}}_1 \cdot \hat{\boldsymbol{\mu}}_2 - 3(\hat{\boldsymbol{\mu}}_1 \cdot \boldsymbol{n})(\hat{\boldsymbol{\mu}}_2 \cdot \boldsymbol{n})}{R^3}\right). \tag{2.1}$$

The strength of the dipole interaction depends on the relative orientation of the dipoles, the distance between them and the magnitude of the dipoles themselves. I will take all the dipoles to be identical and parallel. Depending on the angle between the dipoles and the chain direction, the coupling can be positive or negative. Angles smaller than ≈54.7°, when the dipoles are in a head-to-tail orientation, result in a negative coupling. Such systems are referred to as J-aggregates [21]. Conversely, systems with positive coupling are referred to as H-aggregates. The difference in the sign of the coupling manifests in the spectroscopic differences between J-aggregates and H-aggregates.

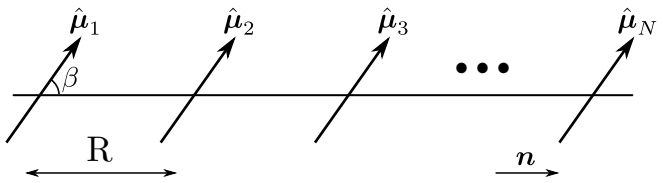

FIGURE 2.1: The arrangement of identical parallel dipoles in the chain. The case $\beta \approx 54.7°$ is shown.

To describe the system quantum mechanically, a basis set of states needs to be decided on. The goal is to describe the diffusive behavior of a single exciton on a chain, ignoring any decay or excitation effects. In the absence of any interactions between sites, the state of the system is fully described by the states of the sites. Every site can either be in the ground state $|g\rangle$ or the excited state $|e\rangle$. The ground state would be given by $|G\rangle = |g, g, g, ..., g\rangle$. This research will investigate systems where only one exciton is present at a time, which simplifies the basis greatly. Such systems can be studied experimentally by using a low powered laser to excite the system to avoid multiple excitation.

The single exciton states will be labeled so $|n\rangle$ represents an exciton localized at site n, for example $|2\rangle = |g, e, g, g, ..., g\rangle$. Every one of these states is associated with an energy ϵ_n which corresponds to the excitation energy of that site. The coupling between sites as a consequence of Eq. is reflected in the off-diagonal terms of the Hamiltonian. This Hamiltonian takes the form

$$\hat{H}_0 = \sum_{i=1}^{N} \epsilon_i |i\rangle \langle i| + \sum_{i \neq j}^{N} J_{ij} |i\rangle \langle j| \,. \tag{2.2}$$

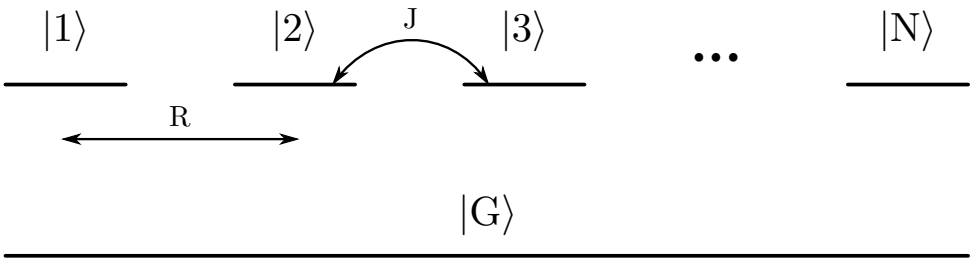

FIGURE 2.2: $|G\rangle$ is the electronic ground state and $|n\rangle$ describes an electronic excitation localized at site n. R is the separation distance between sites. J is the coupling constant connecting neighboring excitation states [22].

For simplicity, only sites directly adjacent to each other will interact (nearest neighbor approximation). The long range dipole-dipole resonant interactions do not change the results significantly and can therefore be neglected. An advantage of this approximation is that it will be easier to diagonalize this tridiagonal Hamiltonian which will be made use of during the calculations. The coupling constant now becomes

$$J_{ij} = (\delta_{i,j+1} + \delta_{i,j-1})J \,. \tag{2.3}$$

The strength of the coupling is taken to be a constant J. Because the models that are used are only valid for the high temperature case, the sign of J is unimportant [23] and can therefore be taken as positive. The Hamiltonian of the model system so far is then

$$\hat{H}_0 = \sum_{i=1}^{N} \epsilon_i |i\rangle \langle i| + \sum_{j=1}^{N-1} J\Big(|j\rangle \langle j+1| + |j+1\rangle \langle j| \Big) \,. \tag{2.4}$$

If the chain is homogeneous, all the site energies are equal. The energies can then be re-scaled so that the first sum in Eq. (2.4) equals 0. However, in practice the transition energies will show a Gaussian spread with variance σ_s^2 around the average.

This static disorder causes excitons to become localized on finite regions of the chain which affects the transport properties. Both cases will be investigated in this thesis.

The above Hamiltonian is valid for an isolated, static system. In real systems, the system interacts with an environment, which adds a time-dependent fluctuating component to the site energies as will be discussed in the next section.

2.1.2 Thermal bath

For excitation energy transfer to take place, it is crucial for the system to be subject to thermal noise. In the absence of such noise, excitons are completely delocalized over the entire chain, meaning the exciton wave functions are and will remain coherent over the whole chain. For transport phenomena, dephasing of coherences is crucial. The coherences are described by the density matrix which is defined as

$$\hat{\rho} = |\psi\rangle \langle\psi| \tag{2.5}$$

where $\langle\psi|$ is the wave function describing the system. This is valid when looking at one chain, i.e. the state is pure and not some ensemble. The matrix elements are given by

$$\rho_{kl} = \langle k| \hat{\rho} |l\rangle = c_k^*(t) c_l(t) \tag{2.6}$$

where $|k\rangle$ and $|l\rangle$ are the energy eigenstates with energies E_k and E_l. The coherences of this state are the off-diagonal elements of this matrix. For an isolated system, the Hamiltonian equals H_0 and does not depend on time. The time-dependence of the coefficients is then trivial and follows from the time-independent Schrödinger equation, $c_k(t) = e^{-iE_k t/\hbar} c_k(0)$. The coherences in this case oscillate like $\rho_{kl} = c_k^*(0) c_l(0) e^{-i\omega_{kl} t}$. Thus, without dephasing an exciton state will oscillate back and forth between the same states indefinitely.

For open quantum systems, coupling to the environment causes dissipation much like the dissipation due to air resistance in a pendulum system. Dissipation arises due to the coupling of the system to additional degrees of freedom such that energy can be transferred to them irreversibly. In practice, it is impossible to model or observe all these environmental degrees of freedom. However, it is possible to model the net effect of the unknown degrees of freedom.

A suitable model that is simple and limits the degrees of freedom is the over-damped Brownian oscillator model [24]. It can be proven that such an environment gives rise to dissipation [25–27]. In this model, the system is bilinearly coupled to a bath consisting of a continuous distribution of independent harmonic oscillators. The coupling strength of each oscillator is dependent on the frequency of the harmonic mode. The bath coupling leads to dephasing of exciton coherences because of those states being coupled to a continuum of states associated with the harmonic modes.

The Hamiltonian of the oscillator model consists of three parts:

$$H = H_S + H_B + H_{SB}\,. \tag{2.7}$$

H_S is the Hamiltonian of the isolated system, H_B describes the bath and H_{SB} the

coupling between the system and the bath. For a particle coupled to a discrete distribution of harmonic normal modes, the Hamiltonians are [28]

$$H_S = \frac{\hat{p}^2}{2M} + V(q) \tag{2.8a}$$

$$H_B = \sum_j \left(\frac{\hat{p}_j^2}{2m_j} + \frac{1}{2} m_j \omega_j^2 \hat{x}_j^2 \right) \tag{2.8b}$$

$$H_{SB} = -\hat{q} \sum_j c_j x_j + \hat{q}^2 \sum_j \frac{c_j^2}{2m_j\omega_j} \,. \tag{2.8c}$$

Here $\hat{p}$ is the system momentum and $\hat{q}$ its conjugate coordinate, $\hat{p}_j$ and $\hat{x}_j$ are those of the bath. The bilinear coupling in the first term of H_{SB} has a strength of c_j. The second term in H_{SB} is a renormalization term that does not depend on the system coordinates.

In the limit of an infinite amount of oscillators, the bath is described by a density of states $W(\omega)$ and a frequency-dependent coupling strength $c(\omega)$. The spectral density $D(\omega)$ is proportional to the product of $W(\omega)$ and $c(\omega)$ and it is often used to specify which model is used. For the underdamped Brownian oscillator model, the spectral density is that of the Drude model [24]

$$D(\omega) = 2\lambda \frac{\omega\Lambda}{\omega^2 + \Lambda^2} \,. \tag{2.9}$$

λ is the reorganization energy that reflects the overall coupling strength of bath to system. This spectral density is Ohmic (linear) for low frequencies with a cut-off for high frequencies. As will become apparent, Λ is the inverse timescale of the dynamics. Note that this is the model for a *colored* noise bath.

To incorporate this model into the simulation for the thesis, the Brownian oscillator model can be formulated as a stochastic model. The effect of the oscillator bath is to randomly push the system, giving rise to a fluctuation of the site energies. These fluctuations are characterized by the time auto-correlation function of the site energies. For the spectral density of Eq. (2.9) the correlation function decays exponentially with rate Λ and there is no inter-site correlation [29]:

$$\langle \delta\epsilon_k(t)\delta\epsilon_l(0)\rangle = \delta_{kl}\sigma^2 \exp(-\Lambda t) \,. \tag{2.10}$$

ϵ_k denotes the energy of site k and its fluctuations around the mean are $\delta\epsilon_k = \epsilon_k - \langle\epsilon_k\rangle$. σ^2 is the variance of the fluctuations and $\Lambda = \frac{1}{\tau_c}$ characterizes the speed of the dynamics, i.e. the 'memory' of the fluctuations. δ_{kl} is the Kronecker delta. The subscript will be dropped to focus on the case of a single site. To generate realizations of fluctuations, an incremental expression can be formulated [30] such that the correlation function obeys Eq. (2.10). First, postulate that the form of the equation is

$$\delta\epsilon(t + \Delta t) = a\delta\epsilon(t) + bG(\sigma) \,. \tag{2.11}$$

$G(\sigma)$ is a random number from a Gaussian distribution with width σ. It is apparent that $\delta\epsilon(t)$ is not fully Markovian, with a memory determined by a. By substituting Eq. (2.11) into Eq. (2.10) the coefficients can be determined and the trajectory is given by

$$\delta\epsilon(t + \Delta t) = \delta\epsilon(t) \exp(-\Lambda\Delta t) + \sqrt{1 - \exp(-2\Lambda\Delta t)} G(\sigma) \,. \tag{2.12}$$

The full Hamiltonian of the system coupled to a thermal bath is then

$$H(t) = H_0 + V(t) = \sum_{i=1}^{N} (\epsilon_i + \delta\epsilon_i(t)) \left|i\right\rangle \left\langle i\right| + \sum_{j=1}^{N-1} J\Big(\left|j\right\rangle \left\langle j+1\right| + \left|j+1\right\rangle \left\langle j\right| \Big) . \quad (2.13)$$

HSR limit

The Haken-Strobl-Reineker model is a limiting case of the model described above. In the limit of very fast bath dynamics ($\Lambda^{-1} \to 0$), the spectral density becomes

$$D(\omega) = 2\lambda \frac{\omega}{\Lambda} \quad (2.14)$$

This linear form is often called white noise. Infinitely fast dynamics also imply that the site energy fluctuations become fully Markovian and all memory is lost. Since the spectral density of the bath is broad compared to the bandwidth of the excitons, the system tends to an equilibrium where every eigenstate of H_0 is equally populated. This is equivalent to the high temperature limit. Hence, the two main limitations to the model are that it is only valid when $k_B T \gg \hbar\Lambda$ and $k_B T \gg \Delta W$ where ΔW is the exciton bandwidth.

The correlation function in the HSR model becomes a delta function:

$$\langle \delta\epsilon_i(t) \delta\epsilon_j(0) \rangle = \delta_{ij} \frac{\sigma^2}{\Lambda} \delta(t) . \quad (2.15)$$

It becomes evident that the fluctuations are fully described by the quantity

$$\Gamma \equiv \frac{\sigma^2}{\hbar^2 \Lambda} . \quad (2.16)$$

Γ is equal to the dephasing (relaxation) rate of the coherences between sites (ρ_{kl}). It is also equal to twice relaxation rate of a single-molecule transition, also known as the homogeneous line width.

For convenience, one can define the dimensionless parameter κ to characterize the speed of the bath dynamics

$$\kappa \equiv \frac{\hbar\Lambda}{\sigma} . \quad (2.17)$$

Since the model assumes fast bath dynamics, it is constrained to the fast modulation limit where the bath dynamics are fast compared to the bath coupling strength, i.e. $\kappa \gg 1$.

2.2 Quantum mechanical evolution operator

The fundamental idea of this thesis is rooted in (non-relativistic) quantum mechanics. To start, the basic concepts are reiterated here. At the basis lies the time-dependent Schrödinger equation:

$$i\hbar \frac{\partial}{\partial t} \left|\psi(\vec{r}, t)\right\rangle = \hat{H}(t) \left|\psi(\vec{r}, t)\right\rangle . \quad (2.18)$$

The evolution of the quantum wave function ψ is determined by the effect of the Hamiltonian operator, $\hat{H}$, on the wave function. Here the Dirac notation is used such that $\langle\psi|\psi\rangle = \int \psi^* \psi \, d^3\vec{r}$.

2.2.1 Time-independent Hamiltonian

If the Hamiltonian does not depend explicitly on time, one can build the solutions to the Schrödinger equation with wave functions of the form $\psi(\vec{r},t) = \chi(\vec{r})\varphi(t)$, which results in the energy basis wave functions:

$$|\psi_n(\vec{r},t)\rangle = e^{-iE_nt/\hbar}\,|\psi_n(\vec{r},0)\rangle\ . \tag{2.19}$$

ψ_n is the wave function for the state with constant energy E_n. The time dependence of the wave function is trivial in this case and fully contained in the phase factor. Any wave function can be expressed in this basis as

$$|\psi(\vec{r},t)\rangle = \sum_k c_k(t)\,|\psi_k(\vec{r},0)\rangle \tag{2.20}$$

where $c_k(t) = \exp(-iE_kt/\hbar)c_k(0)$. Eq. (2.19) suggests that there is an operator that evolves the wave function in time. It can be derived by considering an operator $\hat{U} = e^{-i\hat{H}t/\hbar}$ which commutes with the Hamiltonian. From Hermiticity of the Hamiltonian, $\hat{U}^\dagger = e^{i\hat{H}t/\hbar} = \hat{U}^{-1}$. Multiplying the Schrödinger equation from the left with $\hat{U}^{-1}$ results in

$$\begin{aligned} e^{i\hat{H}t/\hbar}i\hbar\frac{\partial}{\partial t}\,|\psi(\vec{r},t)\rangle &= e^{i\hat{H}t/\hbar}\hat{H}\,|\psi(\vec{r},t)\rangle \\ \frac{\partial}{\partial t}\left[e^{i\hat{H}t/\hbar}\,|\psi(\vec{r},t)\rangle\right] &= 0\,. \end{aligned} \tag{2.21}$$

After integration from t_0 to t one ends up with

$$|\psi(\vec{r},t)\rangle = e^{-i\hat{H}(t-t_0)/\hbar}\,|\psi(\vec{r},t_0)\rangle = \hat{U}(t,t_0)\,|\psi(\vec{r},t_0)\rangle\ . \tag{2.22}$$

So, for a Hamiltonian without an explicit time dependence the time evolution operator is

$$\hat{U}(t,t_0) = e^{-i\hat{H}(t-t_0)/\hbar}$$

which has the properties that it commutes with the Hamiltonian and is unitary. Since $\hat{U}(t,t_0) = \hat{U}^\dagger(t_0,t)$, $\hat{U}^\dagger$ is often called the time reversal operator.

2.2.2 Time-dependent Hamiltonian

For a Hamiltonian that contains an explicit time dependence, the evolution operator is harder to derive. There still exists a time evolution operator such that $|\psi(\vec{r},t)\rangle = U(t,t_0)\,|\psi(\vec{r},t_0)\rangle$ because the Schrödinger equation is a linear partial differential equation in time. A general solution for $\hat{U}$ can be found by substituting Eq. (2.22) into Eq. (2.18) and dividing out the constant $|\psi(\vec{r},t_0)\rangle$. The result is

$$i\hbar\frac{\partial}{\partial t}\hat{U}(t,t_0) = \hat{H}(t)\hat{U}(t,t_0)\,. \tag{2.23}$$

This expression can be directly integrated in time and repeatedly substituted into itself, yielding the result [31]:

$$\begin{aligned}\hat{U}(t,t_0) = 1 &+ \left(\frac{-i}{\hbar}\right)\int_{t_0}^{t} d\tau \hat{H}(\tau) \\ &+ \left(\frac{-i}{\hbar}\right)^2 \int_{t_0}^{t} d\tau \int_{t_0}^{\tau} d\tau' \hat{H}(\tau)\hat{H}(\tau') \\ &+ \left(\frac{-i}{\hbar}\right)^3 \int_{t_0}^{t} d\tau \int_{t_0}^{\tau} d\tau' \int_{t_0}^{\tau'} d\tau'' \hat{H}(\tau)\hat{H}(\tau')\hat{H}(\tau'') \\ &+ \dots\end{aligned} \tag{2.24}$$

$$\hat{U}(t,t_0) \equiv \exp_+\left[\frac{-i}{\hbar}\int_{t_0}^{t} \hat{H}(\tau)d\tau\right]. \tag{2.25}$$

2.3 Numerical integration of the Schrödinger equation

In practice, Eq. (2.25) is not easy to solve. The exponential usually cannot be truncated because convergence is slow. In this thesis I will opt for an alternative approach based on Eq. (2.22) where the wave function evolution is calculated by direct numerical integration of the Schrödinger equation (NISE) [32].

The wave function can be written in terms of some choice of basis states, which is described by Eq. (2.20). This can be substituted into the Schrödinger equation and the constant ket $|\psi_i(\vec{r},0)\rangle$ can be divided out to obtain a differential equation for the wave function coefficients. In matrix form:

$$\frac{\partial}{\partial t}\vec{c}(t) = -\frac{i}{\hbar}\boldsymbol{H}(t)\vec{c}(t)\,. \tag{2.26}$$

This equation can be directly integrated if the Hamiltonian is constant in time. This is approximately true for small enough time intervals. The integration result for one time interval of length Δt is

$$\vec{c}(t+\Delta t) = \exp\left(-\frac{i}{\hbar}\boldsymbol{H}(t)\Delta t\right)\vec{c}(t)\,. \tag{2.27}$$

The time evolution operator is then

$$\boldsymbol{U}(t+\Delta t, t) = \exp\left(-\frac{i}{\hbar}\boldsymbol{H}(t)\Delta t\right). \tag{2.28}$$

and the full evolution of the system over N total time steps is obtained by consecutive multiplication for single time step operators:

$$\boldsymbol{U}(t,0) = \prod_{j=0}^{N-1} \boldsymbol{U}((j+1)\Delta t, j\Delta t)\,. \tag{2.29}$$

Here $t = N\Delta t$. The time evolution operator can also be used to calculate how other operators evolve in time as is the case in the Heisenberg picture:

$$\boldsymbol{A}(t) = \boldsymbol{U}^{\dagger}(t,0)\boldsymbol{A}(0)\boldsymbol{U}(t,0)\,. \tag{2.30}$$

This is useful later on when doing calculations on the system.

It is important to mention the drawbacks of using this method. Like the HSR model, the NISE method is also constrained to the high temperature case ($k_BT \gg \hbar\Lambda$ and $k_BT \gg \Delta W$) since the system will tend to the same uniformly populated equilibrium due to the classical treatment of the bath [32]. However, it is not constrained to the fast modulation limit like the HSR model is. Furthermore, due to the matrix exponentiation and multiplication required the time complexity is $\mathcal{O}(N^3)$ causing calculations for large chains to quickly become unfeasible.

2.3.1 Matrix exponential

The time evolution operator is obtained from the matrix exponential in Eq. (2.28). Calculating a matrix exponential is generally not computationally cheap. It is worth taking a closer look to see how this can be done more efficiently. At a glance, one could use a general purpose algorithm like the scaling-and-squaring method combined with Padé approximants [33, 34] to calculate the exponential. However, the Hamiltonian that is used for these simulations has some properties that allow for a faster calculation.

The Hamiltonian is Hermitian, since $\boldsymbol{H} = \boldsymbol{H}^\dagger$. The spectral theorem for Hermitian matrices states that for an Hermitian matrix $\boldsymbol{H}$ there exists an orthonormal basis consisting of its eigenvectors, which implies that such matrices are diagonalizable. The diagonalization can be expressed as

$$\boldsymbol{H} = \boldsymbol{V}\boldsymbol{\Lambda}\boldsymbol{V}^{-1} \tag{2.31}$$

where $\boldsymbol{V}$ is the matrix with the (orthonormal) eigenvectors of $\boldsymbol{H}$ as its columns and $\boldsymbol{\Lambda}$ is the diagonal matrix with the eigenvalues of $\boldsymbol{H}$ on its diagonal. Hence $\boldsymbol{V}$ is unitary, meaning $\boldsymbol{V}\boldsymbol{V}^\dagger = \boldsymbol{I}$. Now multiply Eq. (2.31) by $-\frac{i}{\hbar}\Delta t$ and then exponentiate, using Taylor series definition of the exponential. It follows that

$$\exp\left(-\frac{i}{\hbar}\boldsymbol{H}\Delta t\right) = \boldsymbol{V}\exp\left(-\frac{i}{\hbar}\boldsymbol{\Lambda}\Delta t\right)\boldsymbol{V}^\dagger\,. \tag{2.32}$$

Since $\boldsymbol{\Lambda}$ is a diagonal matrix, the diagonal values can simply be exponentiated in place to obtain the matrix exponential.

One can then use an eigensolver algorithm that specializes in Hermitian matrices followed by two matrix multiplications, resulting in an overall faster procedure than if using a general purpose exponentiating algorithm. Additionally, since the Hamiltonian of the model is a tridiagonal matrix, calculating the eigenvalues can be made more efficient by using an algorithm that works specifically on tridiagonal matrices.

2.4 Diffusion calculation

There are two different ways in which exciton diffusion is calculated in this research. The first approach is a quantum analogue of classical diffusion. The second method uses the quantum probability flux operator. Both methods are explained below.

2.4.1 Mean-square displacement

In classical physics, the rate at which the particle spreads out around its starting position is related to the diffusion constant. For a classical particle undergoing Brownian motion in one dimension, the mean-square displacement (MSD) is related to the

diffusion coefficient by

$$\lim_{t\to\infty} \langle (x - x_0)^2 \rangle = 2Dt\,. \tag{2.33}$$

The quantum exciton diffusion can be calculated by extending this principle to the excitonic wave function. In the site basis, an exciton can be seen as a quasi-particle with a quantum probability density for its position. To study the diffusion, one can start with a fully localized exciton at position x_0 in the middle of the aggregate. The evolution of the wave function can then be simulated using the NISE method to propagate the starting wave function using Eq. (2.28). For every time step, the MSD can then be calculated. Just like a particle undergoing Brownian motion, the exciton will diffuse over the sites of the aggregate.

For a system with no static disorder, the MSD typically starts out quadratically, signifying ballistic motion, and then rises linearly on longer timescales. The diffusion constant can be calculated by fitting a linear function to the tail of the MSD evolution.

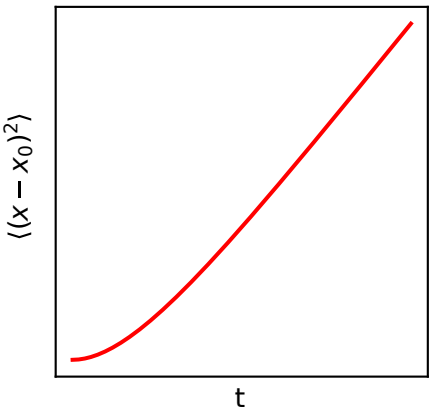

FIGURE 2.3: MSD over time, averaged over many trajectories of the Hamiltonian.

The simulation model is stochastic and the Hamiltonian therefore incorporates random noise. The MSD values need to be averaged to account for this. To achieve this, the system is evolved from the start for many realizations of random numbers and the MSD is then averaged over these realizations.

To calculate the MSD for a single evolution, it is necessary to calculate the expectation value of the operator $(\hat{x} - x_0)^2$. x_0 is chosen such that it is in the middle of the chain. If there are N total sites (and N is odd) and the first site is at $x = R$, the middle is $x_0 = \frac{N+1}{2}R$ where R is the inter-site distance. Here x is the position operator with the following eigenvalues: $\hat{x}\,|n\rangle = nR\,|n\rangle$. Using this we can work out the MSD operator. Its matrix elements are

$$(\hat{x} - x_0)^2_{ij} = \langle i|\,(\hat{x} - x_0)^2\,|j\rangle = \big((iR)^2 - 2iRx_0) + x_0^2\big)\delta_{ij}\,. \tag{2.34}$$

As expected, the MSD is 0 for the state where the exciton is localized at x_0.

To get a value for the diffusion, $\langle (x - x_0)^2 \rangle = 2Dt$ is fitted to the linear tail of the simulation data. It is only possible to get a good fit if the evolution is long enough for the linear tail to become well defined. The simulation time step is constrained by the correlation time: $\Delta t \ll \Lambda^{-1} = \tau_c$. If the diffusion is too slow, it will take a long time to simulate the evolution until the MSD becomes linear. Furthermore the noisiness

(and therefore the fit) of the MSD depends on the amount of realizations that are averaged over. This is a trade-off between speed and accuracy.

Edge effects

For small chains or long times, the exciton diffusion will reach the edge of the chain. When this happens, the wave function will have no more new sites to spread to and the MSD will begin to level off.

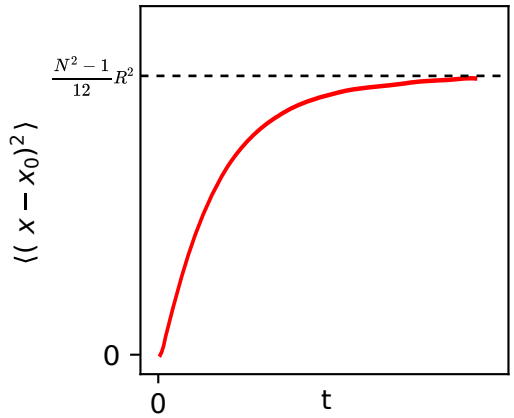

FIGURE 2.4: Saturation is reached after diffusion over large time scales.

The asymptotic maximum value of the MSD is reached when the exciton diffuses uniformly across all sites and equilibrium is reached, so the wave function coefficients will be

$$\lim_{t\to\infty} |c_m(t)|^2 = \lim_{t\to\infty} |c_n(t)|^2 = \text{constant} \tag{2.35}$$

and since $\sum_{k=1}^{N} |c_k(t)|^2 = 1$, we have

$$\lim_{t\to\infty} |c_m(t)|^2 = \frac{1}{N}\,. \tag{2.36}$$

The wave function is then

$$|\psi_{eq}\rangle = \sum_{k=1}^{N} \frac{e^{-i\phi_k}}{\sqrt{N}} |k\rangle \tag{2.37}$$

where $e^{-i\phi_k}$ is an unknown phase factor.

The asymptotic MSD value can now be calculated using $x_0 = \frac{N+1}{2}$:

$$\begin{aligned}\lim_{t\to\infty}\langle(\hat{x}-x_0)^2\rangle &= \langle\psi_{eq}|\,(\hat{x}-x_0)^2\,|\psi_{eq}\rangle = \sum_{k,l=1}^{N}\langle k|\,\frac{e^{i\phi_k}}{\sqrt{N}}(\hat{x}-x_0)^2\frac{e^{-i\phi_l}}{\sqrt{N}}\,|l\rangle \\ &= \frac{1}{N}\sum_{l=1}^{N}\left((lR)^2-2x_0lR+x_0^2\right) \\ &= \frac{R^2}{N}\left(\frac{N(N+1)(2N+1)}{6}-2\left(\frac{N+1}{2}\right)\left(\frac{N(N+1)}{2}\right)+N\left(\frac{N+1}{2}\right)^2\right) \\ &= \frac{N^2-1}{12}R^2\,.\end{aligned} \tag{2.38}$$

This is also confirmed by the simulations. It is possible to make a rough estimate on when the edge effects start to become significant. In parallel to diffusion for a classical particle, the MSD can be equated to the variance of a Gaussian distribution signifying the position spread of the exciton. It is reasonable to assume edge effects start to come into play when the 3σ tails reach the chain edges: $3\sigma_t \approx \frac{N}{2}R$. Therefore the MSD will start transitioning around

$$\langle(\hat{x}-x_0)^2\rangle_t = \frac{N^2}{36}R^2\,. \tag{2.39}$$

To ensure this limit is not crossed, the chain length can be increased or the evolution time decreased.

2.4.2 Quantum Green-Kubo expression

Instead of calculating the diffusion using the MSD, it can be calculated in an alternative fashion using an expression derived from the Green-Kubo formula. For a one-dimensional classical system, this equation connects the integral two-time velocity auto-correlation function to the diffusion constant [35]:

$$D = \int_0^\infty \langle v(t)v(0)\rangle dt\,. \tag{2.40}$$

For a quantum system like the one in this thesis, the Green-Kubo relation involves the quantum flux operator which serves as the quantum analogue of velocity. The flux operator is defined as the time derivative of the exciton position operator [23]:

$$\hat{j}(\boldsymbol{u}) = \frac{i}{\hbar}\sum_{n,m}(\boldsymbol{u}\cdot\boldsymbol{r}_{nm})\,J_{nm}\,|m\rangle\,\langle n|\,. \tag{2.41}$$

$\boldsymbol{u}$ is the unit vector along which the diffusion will be calculated and $\boldsymbol{r}_{nm}$ the vector connecting sites n and m. In the quantum case, the correlation function takes a trace of the product of operators, combined with a thermal average [36]. The Green-Kubo relation for the exciton diffusion is then [15]

$$D(\boldsymbol{u}) = \frac{1}{Z_s}\int_0^\infty dt\ \mathrm{Tr}[e^{-\beta\hat{H}_s}\hat{j}(\boldsymbol{u},t)\hat{j}(\boldsymbol{u})]\,. \tag{2.42}$$

Here Z_s is the statistical mechanical partition function of the system, $Z_s = \sum_i e^{-\beta E_i}$, $\beta = \frac{1}{k_B T}$ and H_s the system Hamiltonian. For the calculation, the high temperature limit is taken in accordance with the HSR model. This implies that the partition function $Z_s = N$ and $\beta = 0$. It is important to note that the integral will need to be performed for disorder realizations of the Hamiltonian and then averaged, just like with the MSD.

The method of obtaining the integrand of the Green-Kubo relation is similar to the previous section. NISE is used to calculate the evolution of the flux operator according to Eq. (2.30):

$$\hat{j}(\boldsymbol{u}, t) = \hat{U}^{\dagger}(t, 0)\hat{j}(\boldsymbol{u}, 0)\hat{U}(t, 0)\,. \tag{2.43}$$

The time evolution operator is calculated with $\Delta t \ll \Lambda^{-1}$.

To be able to numerically evaluate the improper integral, the integrand must be well behaved. For typical parameters, the integrand tends to zero nicely for large values of t. This allows for the approximation where the integral is truncated for high values of t where the integrand vanishes.

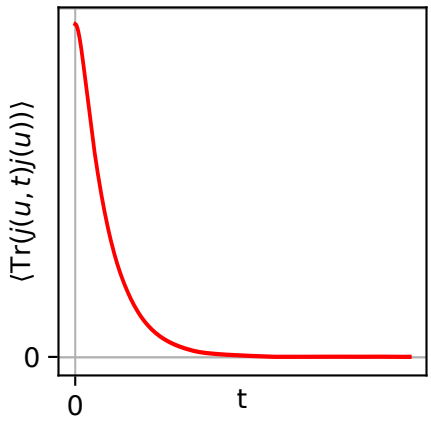

FIGURE 2.5: The integrand of the Green-Kubo relation, Eq. (2.42), averaged over many trajectories of the Hamiltonian.

2.4.3 HSR Model analytic solution

The MSD and Green-Kubo relation calculations are compared to the HSR model diffusion. Under the assumptions of this model it is possible to derive an analytical expression for the diffusion starting from the Green-Kubo relation defined in Eq. (2.42). The evolution of the flux operator is described by the Heisenberg equation of motion combined with an exponential relaxation with rate Γ [15]:

$$\hat{j}(\boldsymbol{u}, t) = e^{\frac{i}{\hbar}\hat{H}_0 t}\hat{j}(\boldsymbol{u}, 0)e^{-\frac{i}{\hbar}\hat{H}_0 t}e^{-\Gamma t} \tag{2.44}$$

where $\hat{H}_0$ is the unperturbed Hamiltonian containing (if present) the static disorder. When combined with Eq. (2.42) and transforming to the eigenbasis of $\hat{H}_0$ the analytical

expression for the diffusion becomes

$$D(\boldsymbol{u}) = \frac{1}{N} \sum_{\mu,\nu=1}^{N} \frac{\Gamma}{\Gamma^2 + (E_{\mu\nu}/\hbar)^2} \left| \hat{j}_{\mu\nu}(\boldsymbol{u}) \right|^2 . \tag{2.45}$$

Here $E_{\mu\nu} = E_\mu - E_\nu$ is the energy difference between eigenstates μ and ν, and $\hat{j}_{\mu\nu}$ is the flux operator in the energy eigenbasis, calculated by

$$\hat{j}_{\mu\nu}(\boldsymbol{u}) = \hat{\boldsymbol{V}}^\dagger \hat{j}_{mn}(\boldsymbol{u}) \hat{\boldsymbol{V}} \tag{2.46}$$

where $\hat{\boldsymbol{V}}$ is the matrix with the eigenvectors of $\hat{H}_0$ as its columns (the matrix that diagonalizes $\hat{H}_0$). It is important to note that if there is static disorder, the diffusion needs to be averaged over many realizations of static disorder. The power of Eq. (2.45) lies in the fact that it is not necessary to explicitly evolve the Hamiltonian with its dynamic disorder. The dynamic disorder is captured in a single parameter, Γ. Because of this, only one matrix diagonalization is needed to calculate D whereas for the MSD, Eq. (2.33), and Green-Kubo integral, Eq. (2.42), this needs to be done many times, one for every time step. It is therefore feasible to simulate much larger chains with the HSR model.

In the limit of an infinite homogeneous chain (no static disorder) with only nearest-neighbor interactions the diffusion can be derived [23] as

$$D_{\text{hom}} = \frac{2R^2 J^2}{\hbar^2 \Gamma} . \tag{2.47}$$

This expression is expected to hold for finite chains as long as $2\pi J/N \ll \hbar\Gamma$, further simplifying calculations in this regime.

Chapter 3

Results

In this section, the diffusion is calculated using three different methods as a function of the bath parameters σ and Λ. Eqs. (2.33) and (2.42) are compared to the HSR model, Eq. (2.45). The main focus is on homogeneous chains, i.e. the static disorder σ_s equals zero. One choice of static disorder will be considered after.

In order to test the NISE-derived methods for calculating the exciton diffusion, the parameter range to simulate has to be carefully selected. This must be done such that the model can be compared with the HSR model. As stated in Section 2, the HSR model assumes a white noise heat bath. In the context of the tested model, this effectively means that $\Lambda^{-1} \to 0$ and $\kappa \gg 1$. It is therefore expected that the NISE diffusion calculations agree with the HSR model for these parameter regimes.

The diffusion calculations for the MSD and Green-Kubo methods were done using a parallelized program written in C++, utilizing the Eigen [37] library for linear algebra operations. The program was parallelized so multiple trajectories can be calculated simultaneously. The calculations were performed by the Peregrine HPC cluster of the University of Groningen.

The chain length for each set of parameters was chosen to provide a balance between performance and accuracy. The diffusion constant is independent of N as long as both methods are well behaved for that particular choice of N. Furthermore, for every calculation the value $J = 300\ \mathrm{cm}^{-1}$ was used and every other parameter was defined relative to J.

3.1 Homogeneous chain

In figure 3.1 the diffusion constant D as a function of Γ was numerically calculated and plotted in log-log. The value of κ was fixed to 1 and so the parameters vary from $\hbar\Gamma = \sigma = \hbar\Lambda = 0.1J$ to $\hbar\Gamma = \sigma = \hbar\Lambda = 10J$. The choice of $\kappa = 1$ corresponds to the intermediate modulation regime. Fixing κ allows one to see the potential shortcomings of the white noise HSR model compared to the colored noise models.

The general features of all models match well, with a monotonic decrease as Γ increases. The HSR model follows a straight line, corresponding with -1 exponent of Γ in Eq. (2.47). This is expected since the condition $2\pi J/N \ll \hbar\Gamma$ was true for every point. Note that the MSD and Green-Kubo methods agree with each other well on this range of parameters. The difference between the two at low Γ is caused by edge effects and convergence problems if the dynamics are slow and the dynamic disorder is small.

Looking at the behavior at low Γ it becomes evident that the HSR model underestimates the diffusion in this regime. This signifies that a colored noise bath is more effective at inducing diffusion than white noise at low $\Gamma/\Lambda/\sigma$.

Finally, note that while the independent variable used was Γ, due to the fixing of κ it is the same as Λ or $\sigma/\hbar$. This explains why the models converge for high Γ;

As Γ increases, so does Λ and the white noise limit is approached so that the HSR model becomes valid again. It is an encouraging result that the MSD and Green-Kubo formulae agree with the HSR model in this limit, showing that indeed the colored noise models reduce to the white noise model for $\Lambda^{-1} \to 0$.

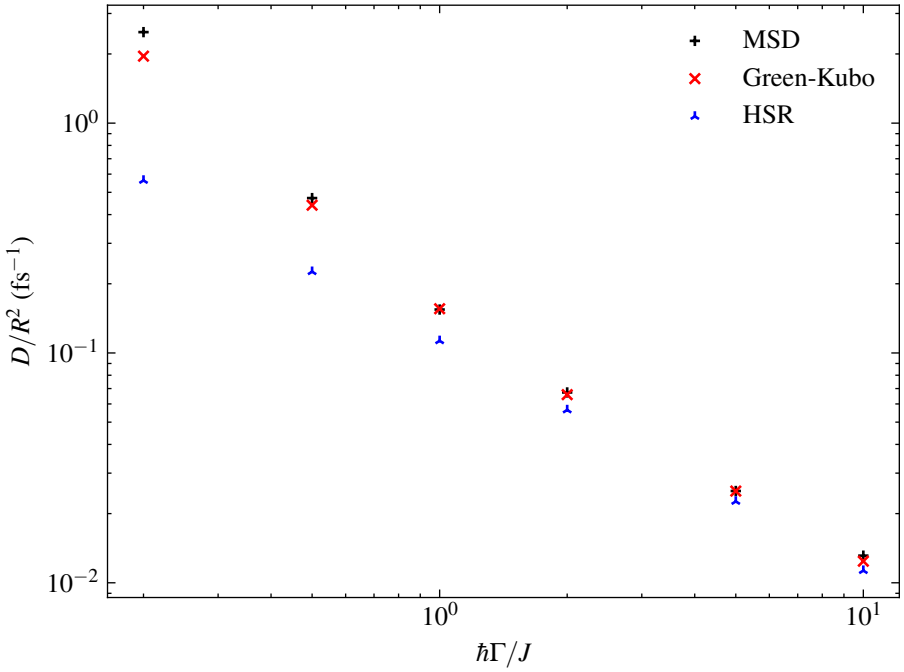

FIGURE 3.1: Diffusion constant for $\kappa = 1$. As a result, $\Gamma = \Lambda = \sigma/\hbar$.

Next, using the three models, the diffusion constant was calculated for a single value of Γ while varying σ and Λ and plotted log-log in figure 3.2. This way of varying the parameters has the same effect as varying the modulation strength κ, illustrated by the conversion table 3.1. Note that since Γ is fixed the HSR model yields the same value for every choice of σ and Λ. The effect of colored noise can now be seen for each modulation regime.

In the slow modulation limit, the HSR model gives a lower value for the diffusion, with the difference increasing as κ goes lower. This is expected since the HSR is only valid in the fast modulation limit. The colored bath diffusion models decrease monotonically over the sampled range and appear to converge to a constant value for high κ. Note that the HSR model follows a straight line with slope -1 as expected from Eq. (2.47).

One would expect that the three methods converge for $\kappa \gg 1$ and although both seem to yield a constant diffusion in the limit, the MSD and Green-Kubo methods converge to a lower value. A possible explanation is the way Γ is calculated from σ and Λ to be able to relate to the HSR method. In the MSD and Green-Kubo methods, σ and Λ determine the speed and strength of the fluctuations in the site energies and which are then related to Γ. However, because Γ in the HSR model represents the dephasing rate of the elements ρ_{kl} in the eigenbasis, it relates to the fluctuations in the eigen energies and not the site energies. Thus, there could be some 'effective' dephasing rate, Γ_{eff}, that differs from the quantity $\Gamma = \sigma/\hbar^2\Lambda$. This effective value should then be used to calculate the equivalent HSR diffusion. In this case, since the diffusion constant decreases with Γ, one expects to find that $\Gamma_{\text{eff}} > \Gamma$.

κ	σ/J	$\hbar\Lambda/J$
0.316	0.316	0.1
0.447	0.447	0.2
0.707	0.707	0.5
1	1	1
1.414	1.414	2
2.236	2.236	5
3.162	3.162	10

TABLE 3.1: Conversion key for the parameter values in figures 3.2 and 3.3.

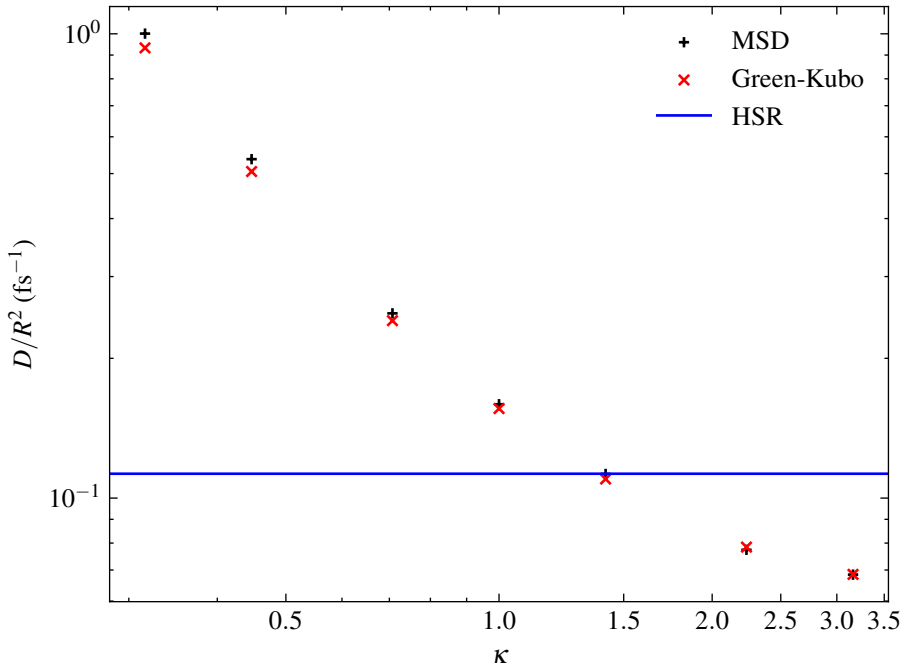

FIGURE 3.2: Diffusion constant for $\hbar\Gamma = J$. σ varies with Λ as $\sigma/J = \sqrt{\hbar\Lambda/J}$

3.2 Static disorder

Finally, the diffusion constant was calculated for a chain containing static disorder. The static disorder was taken to be of intermediate strength: $\sigma_s = J$. The same calculation as done for figure 3.2 was done here but this time the calculations were also averaged over realizations of static disorder. The result is plotted in log-log in figure 3.3.

One immediately observes that calculated diffusion values are much lower than for the homogeneous case. The explanation is simple: the difference in energy of adjacent sites acts like an obstacle for the diffusion. Locally, there will be some site pairs where the energy difference is large compared to the dynamic fluctuations. It then takes time for an exciton to diffuse across such a barrier. Another observation is that there is an optimum for the diffusion now. The optimum appears around $\kappa = \sigma/J = 1$. This coincides with $\sigma_s = \sigma$. In this regime, the fluctuations are strong enough to overcome the barriers of the static disorder, but not too large to hamper the diffusion. After

the optimum is reached, the same decreasing behavior as in the homogeneous case is seen.

Like in figure 3.2 one expects the three methods to agree in the limit of large κ. Again, the HSR model yields a larger value for the diffusion in this limit. This has been commented on in the previous section.

Finally, note that the MSD and Green-Kubo methods do not agree as well for small κ in this plot. The more accurate method is the MSD. This will be explained in the next section.

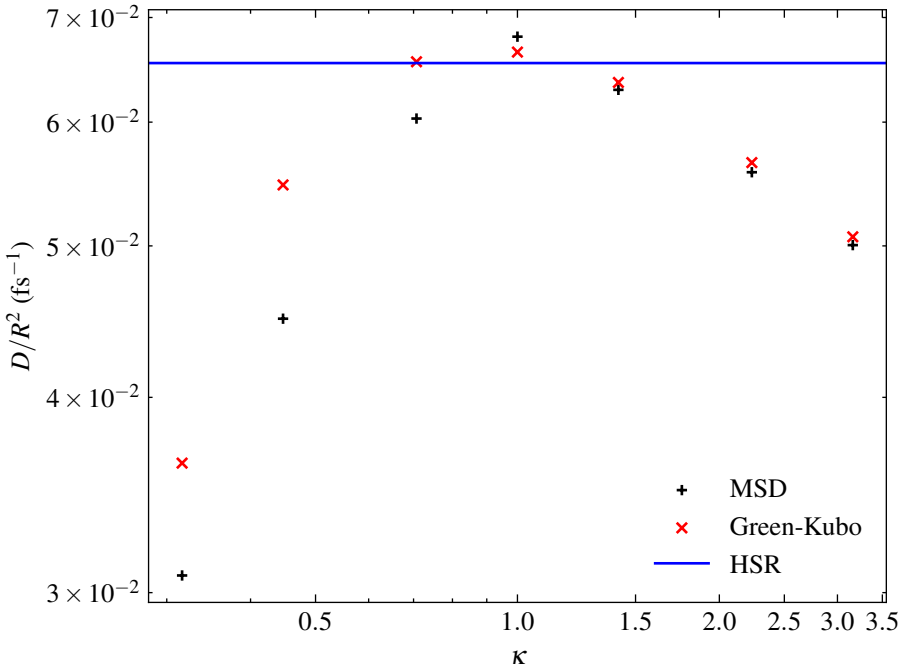

FIGURE 3.3: Diffusion constant for $\hbar\Gamma = J$, with a static disorder $\sigma_s = J$. σ and Λ are varied such that $\sigma/J = \sqrt{\hbar\Lambda/J}$.

3.3 Comparison between colored-noise methods

While the two colored-noise models use the same underpinning propagation method (NISE), they calculate the diffusion in two different ways. The convergence rate and accuracy differ depending on the parameter values. Each method's strengths and weaknesses will be discussed in this section.

3.3.1 MSD method

The accuracy of the MSD method is dependent on how long the diffusion process is run. The diffusion is calculated by fitting a straight line to the tail of the MSD and thus, the longer the diffusion, the better the fit will be and the better the accuracy. The key factor is how long it takes for the MSD to become fully diffusive. In extreme cases where the diffusion starts out slowly, it is possible to run into edge effects before there is enough data for a proper fit. This happens if the fluctuations are small and the dynamics slow. In this case the chain length has to be increased, severely slowing the calculation. For homogeneous chains, there is a saving grace. The MSD in homogeneous chains starts out quadratically in time, corresponding to a ballistic diffusion regime [38]. The functional form for the MSD in absence of edge effects

becomes

$$\langle (x(t) - x_0)^2 \rangle = ab\left(t - a\left[1 - \exp\left(-\frac{t}{a}\right)\right]\right) . \tag{3.1}$$

The entire range can then be fitted to improve accuracy, reducing the need for larger chain sizes.

Another factor is the statistical averaging that has to be performed for the dynamic and static disorder. The fluctuations in the MSD trajectory increase when σ and σ_s are large. To maintain the same level of accuracy, the amount of realizations has to be increased. When both static and dynamic disorder are present the effect is compounded. However, the averaging nature of fitting the slope means that this effect can also be dealt with by increasing the amount of time steps.

3.3.2 Green-Kubo method

The Green-Kubo method can be evaluated by looking at how the integrand of Eq. (2.42) behaves. In the ideal case, the integrand decays to zero quickly so that the integral can be calculated without needing to simulate until large t.

The decay rate of the integrand increases with dynamic disorder, so the required simulation time decreases as σ increases. Interestingly, the speed of the dynamics, Λ, has almost no effect on the integrand decay rate. This is explained by noting that the decay of the integrand is determined by Eq. (2.44). In the eigenbasis, the equation takes the same form. If one thinks about a simple isolated two site system, it is evident that the time evolution will oscillate back and forth. Adding disorder causes dephasing, such that the autocorrelation will go to zero. The rate at which this happens is dependent on the distribution width of the eigenstates, the larger the width the faster the integrand will decay. The width only depends on the dynamic disorder, σ. Only when Λ is very large it could have an effect on the decay since motional narrowing will narrow the eigen energy distributions [39]. Finally, adding static disorder causes the integrand decay rate to further increase.

For a homogeneous chain, the Green-Kubo method is less well behaved when $\sigma \ll J$. Besides a long simulation time, the integrand also overshoots zero and then finally converges to zero from below. This wide trough gets less deep and eventually disappears when the chain size N is increased, although it makes the simulation much more computationally expensive since this method has a time complexity of $\mathcal{O}(N^3)$.

When static disorder is introduced, the trough problem is more severe. For $\sigma < \sigma_s$ it becomes unfeasible time-wise to increase the chain size enough to mitigate the problem, resulting in loss of accuracy. It is better to use the MSD in this range.

Finally, this method also experiences more statistical fluctuations for large σ, especially in the tail of the integrand. This is easily mitigated by running more realizations.

3.3.3 Direct comparison

The fact that both methods give close to the same value for the diffusion constant is an encouraging result. However, it raises the question: which one is best to use?

In terms of computation the Green-Kubo method is slower since it performs matrix multiplications while the MSD method performs matrix-vector multiplications. In the regime where both methods work well, the performance is similar. However, in the breakdown regime for a homogeneous chain, $\sigma \ll J$, the MSD is the better choice. By fitting the ballistic part of the MSD the simulation time is kept short. The Green-Kubo method in this case needs to go to much higher t and N to obtain the same

accuracy, making it slower. For a chain containing static disorder, the Green-Kubo method struggles for $\sigma < \sigma_s$, needing a much higher N than the MSD method which does not have this problem.

The calculations in this thesis were all done for the high temperature limit. The MSD method is based on NISE and there finite temperature effects are not encoded in it. In contrast, the Green-Kubo integral, Eq. (2.42) has a factor to correct for these effects. For calculations incorporating the temperature dependence, the Green-Kubo method then becomes the method of choice.

Chapter 4

Conclusions

4.1 Results and interpretation

In this thesis, the excitation energy diffusion was studied for linear 1D aggregates coupled to a heat bath environment. The sites in the aggregates are coupled in nearest neighbor fashion with coupling strength J, which was kept constant with value $J = 300\ \mathrm{cm}^{-1}$. The interaction of the heat bath with the system gives rise to a net energy transport when a site is excited. The bath is modeled by a continuous distribution of harmonic oscillators, characterized by a spectral density function. The spectral density shape, also referred to as color, is determined by Λ, the inverse timescale of the bath dynamics. The main goal of this thesis is to investigate and compare the effect of colored noise on diffusion as opposed to white noise. The diffusion was calculated and compared between models for various combinations of the static disorder, σ_s, dynamic disorder, σ and dynamics timescale Λ^{-1}.

The diffusion was modeled using two colored noise models and compared to the white noise based Haken-Strobl-Reineker (HSR) model. Both colored noise models used Numerical Integration of the Schrödinger Equation (NISE) to calculate the time evolution of the system. The first model calculated the mean-square displacement (MSD) of a single exciton by evolving the exciton wave function using NISE. The second model used NISE to calculate the auto-correlation of the quantum flux operator, which was then integrated in a quantum Green-Kubo expression. Note that the Green-Kubo method is the more general version of the HSR model.

The simulations were performed by a specially written parallelized computer program that was run on the Peregrine HPC cluster of the University of Groningen. The parameter space was sampled according to three different setups.

For a homogeneous chain, the ratio between dynamic disorder and bath dynamics time scale was kept constant. The MSD and Green-Kubo calculations were plotted along with the HSR calculation. The results showed that the colored noise models agree well with each other. For large Λ the colored and white noise models all agreed as expected. Elsewhere the diffusion was underestimated by the HSR model. The behaviour of the diffusion constant for the three methods is roughly the same: the diffusion monotonically decreases for this parameter range.

To see the effect of decoupling the HSR dephasing rate into disorder strength and inverse dynamics timescale, the dephasing rate was kept constant for the second setup. This resulted in the HSR model giving the same value for the diffusion for every σ/Λ pair chosen this way. On the sampled parameter range, the colored noise models again agreed well. The diffusion decreased with increasing σ and Λ, seemingly converging to a constant value in the white noise limit. Surprisingly, the HSR value did not coincide with the colored noise limiting value. This is possibly explained by the difference between the way Γ is calculated from the site energy fluctuations, while in the HSR model Γ represents the dynamics in the eigenbasis.

In the third scenario, a chain containing static disorder was simulated for a fixed value of Γ. The static disorder was set at $\sigma_s = J$. The diffusion was overall lower than for a homogeneous chain, which is explained by the fact that the static disorder acts like a barrier that an exciton has to overcome to hop to the next site, slowing the diffusion. The diffusion showed an optimum around $\sigma = \sigma_s$. Around this point, the dynamic disorder becomes large enough to overcome the static disorder but not too large to reduce diffusion. The scaling for large σ and Λ is the same as for the homogeneous case. The same argument as for the homogeneous case applies to explain the difference between the convergence value of the colored models versus the HSR model.

A key takeaway from these calculations is the fact that colored noise makes a significant difference for the parameters tested here. The diffusion seems to be significantly underestimated by the HSR model. Therefore, when calculating diffusion away from the white noise limit ($\Lambda \to \infty$) it is important to use a method that incorporates a more general, colored, bath spectral density.

4.2 Outlook

Due to time constraints, only a select few parameters were sampled in this research. Two slices of the parameter space were taken, $\Gamma = \frac{\sigma^2}{\hbar^2 \Lambda} = J$ and $\kappa = \frac{\Lambda}{\sigma} = 1$. Other possible interesting slices could be those at constant σ or Λ, to fully untangle the effects of those two parameters. More extreme parameters regimes could also be explored to give insight into other regimes potentially relevant for light harvesting systems.

The emphasis of this thesis was on homogeneous chains. Only a single value of static disorder was used. It might therefore be worth investigating how the methods scale and compare with a range of values of static disorder present. Additionally, it may be possible to calculate an effective Γ that explains the difference between the colored noise results and the HSR model. This could be done by looking at the eigenstates as they evolve. Finally, using the Green-Kubo integral the temperature dependence of the diffusion can be studied.

Chapter 5

Acknowledgments

Looking back on the process of completing this thesis I have to give credit where credit is due. A big contribution to me finishing this thesis is thanks to all the people who supported me in this endeavor. First, I want to thank my supervisor, Thomas la Cour Jansen, for being very supportive when progress was slow and for having the patience of a saint. He helped put me on the right track and was always available for questions, which has helped me immensely. Secondly, I want to thank my parents. They supported me and spurred me on in my research. Thirdly, I want to thank my second examiner, Anastasia Borschevsky, for agreeing to take on this role on short notice. Finally, I want to thank my friends for all the advice they gave me on how to proceed and all the encouraging words. In particular, I want to thank Debora, who was there by my side for many late nights and has been great at motivating me and reminding me that there was more work to be done.

Bibliography

[1] J. Wu, F. Liu, Y. Shen, J. Cao, and R. J. Silbey, "Efficient energy transfer in light-harvesting systems, I: optimal temperature, reorganization energy and spatial–temporal correlations", New J. Phys. **12**, 105012 (2010).

[2] E. Collini, C. Y. Wong, K. E. Wilk, P. M. G. Curmi, P. Brumer, and G. D. Scholes, "Coherently wired light-harvesting in photosynthetic marine algae at ambient temperature", Nature **463**, 644–647 (2010).

[3] A. B. Doust, K. E. Wilk, P. M. Curmi, and G. D. Scholes, "The photophysics of cryptophyte light-harvesting", J. Photochem. Photobiol. A **184**, 1–17 (2006).

[4] T. Mirkovic, A. B. Doust, J. Kim, K. E. Wilk, C. Curutchet, B. Mennucci, R. Cammi, P. M. G. Curmi, and G. D. Scholes, "Ultrafast light harvesting dynamics in the cryptophyte phycocyanin 645", Photochem. Photobiol. Sci. **6**, 964–975 (2007).

[5] A. W. Roszak, T. D. Howard, J. Southall, A. T. Gardiner, C. J. Law, N. W. Isaacs, and R. J. Cogdell, "Crystal structure of the RC-LH1 core complex from Rhodopseudomonas palustris", Science **302**, 1969–1972 (2003).

[6] G. McDermott, S. M. Prince, A. A. Freer, A. M. Hawthornthwaite-Lawless, M. Z. Papiz, R. J. Cogdell, and N. W. Isaacs, "Crystal structure of an integral membrane light-harvesting complex from photosynthetic bacteria", Nature **374**, 517–521 (1995).

[7] T. Brixner, R. Hildner, J. Köhler, C. Lambert, and F. Würthner, "Exciton Transport in Molecular Aggregates - From Natural Antennas to Synthetic Chromophore Systems", Adv. Energy Mater. **7**, 1700236 (2017).

[8] Y. Qiao, F. Polzer, H. Kirmse, E. Steeg, S. Kühn, S. Friede, S. Kirstein, and J. P. Rabe, "Nanotubular J-Aggregates and quantum dots coupled for efficient resonance excitation energy transfer", ACS Nano **9**, 1552–1560 (2015).

[9] I. Patmanidis, A. H. de Vries, T. A. Wassenaar, W. Wang, G. Portale, and S. J. Marrink, "Structural characterization of supramolecular hollow nanotubes with atomistic simulations and SAXS", Phys. Chem. Chem. Phys. **22**, 21083–21093 (2020).

[10] K. A. Clark, C. W. Cone, and D. A. Vanden Bout, "Quantifying the polarization of exciton transitions in double-walled nanotubular J-Aggregates", J. Phys. Chem. C **117**, 26473–26481 (2013).

[11] B. Kriete, J. Lüttig, T. Kunsel, P. Malý, T. L. C. Jansen, J. Knoester, T. Brixner, and M. S. Pshenichnikov, "Interplay between structural hierarchy and exciton diffusion in artificial light harvesting", Nat. Commun. **10**, 4615 (2019).

[12] Y. Wan, A. Stradomska, J. Knoester, and L. Huang, "Direct imaging of exciton transport in tubular porphyrin aggregates by ultrafast microscopy", J. Am. Chem. Soc. **139**, 7287–7293 (2017).

[13] Y. Tanimura, "Numerically "exact" approach to open quantum dynamics: The hierarchical equations of motion (HEOM)", J. Chem. Phys. **153**, 020901 (2020).

[14] A. Ishizaki and G. R. Fleming, "On the adequacy of the Redfield equation and related approaches to the study of quantum dynamics in electronic energy transfer", J. Chem. Phys. **130**, 234110 (2009).

[15] C. Chuang, C. K. Lee, J. M. Moix, J. Knoester, and J. Cao, "Quantum diffusion on molecular tubes: Universal scaling of the 1D to 2D transition", Phys. Rev. Lett. **116**, 196803 (2016).

[16] H. Fidder, J. Knoester, and D. A. Wiersma, "Optical properties of disordered molecular aggregates: A numerical study", J. Chem. Phys. **95**, 7880–7890 (1991).

[17] R. Augulis, A. Pugžlys, and P. H. M. van Loosdrecht, "Exciton dynamics in molecular aggregates", Phys. Status Solidi C **3**, 3400–3403 (2006).

[18] D. Abramavicius and S. Mukamel, "Exciton dynamics in chromophore aggregates with correlated environment fluctuations", J. Chem. Phys. **134**, 174504 (2011).

[19] M. Manrho, T. L. C. Jansen, and J. Knoester, "Optical signatures of the coupling between excitons and charge transfer states in linear molecular aggregates", J. Chem. Phys. **156**, 224112 (2022).

[20] S. Ravets, H. Labuhn, D. Barredo, L. Béguin, T. Lahaye, and A. Browaeys, "Coherent dipole–dipole coupling between two single Rydberg atoms at an electrically-tuned Förster resonance", Nat. Phys. **10**, 914–917 (2014).

[21] D. Abramavicius, V. Butkus, and L. Valkunas, "Chapter 1 - interplay of exciton coherence and dissipation in molecular aggregates", in *Quantum efficiency in complex systems, part II*, Vol. 85, edited by U. Wüerfel, M. Thorwart, and E. R. Weber, Semiconductors and Semimetals (Elsevier, 2011), pp. 3–46.

[22] C. Warns, I. Barvik, and P. Reineker, "Energy transport and optical line shapes in dimers: Analytical description of the influence of colored noise", Phys. Rev. E **57**, 3928–3936 (1998).

[23] T. Kunsel, T. L. C. Jansen, and J. Knoester, "Scaling relations of exciton diffusion in linear aggregates with static and dynamic disorder", J. Chem. Phys. **155**, 134305 (2021).

[24] S. Mukamel, *Principles of nonlinear optical spectroscopy*, 6 (Oxford University Press on Demand, 1999).

[25] U. Weiss, *Quantum dissipative systems*, Fifth (World Scientific, 2021).

[26] A. J. Leggett, S. Chakravarty, A. T. Dorsey, M. P. A. Fisher, A. Garg, and W. Zwerger, "Dynamics of the dissipative two-state system", Rev. Mod. Phys. **59**, 1–85 (1987).

[27] Y. Yan and R. Xu, "Quantum mechanics of dissipative systems", Annu. Rev. Phys. Chem. **56**, 187–219 (2005).

[28] P. Hänggi and G.-L. Ingold, "Fundamental aspects of quantum Brownian motion", Chaos **15**, 026105 (2005).

[29] A. S. Bondarenko, J. Knoester, and T. L. Jansen, "Comparison of methods to study excitation energy transfer in molecular multichromophoric systems", Chem. Phys. **529**, 110478 (2020).

[30] D. Cringus, T. l. C. Jansen, M. S. Pshenichnikov, and D. A. Wiersma, "Ultrafast anisotropy dynamics of water molecules dissolved in acetonitrile", J. Chem. Phys. **127**, 084507 (2007).

[31] F. J. Dyson, "The Radiation Theories of Tomonaga, Schwinger, and Feynman", Phys. Rev. **75**, 486–502 (1949).

[32] T. l. C. Jansen and J. Knoester, "Nonadiabatic Effects in the Two-Dimensional Infrared Spectra of Peptides: Application to Alanine Dipeptide", J. Phys. Chem. B **110**, 22910–22916 (2006).

[33] N. J. Higham, "The scaling and squaring method for the matrix exponential revisited", SIAM J. Matrix Anal. Appl. **26**, 1179–1193 (2005).

[34] N. J. Higham and A. H. Al-Mohy, "Computing matrix functions", Acta Numer. **19**, 159–208 (2010).

[35] R. Kubo, "Statistical-mechanical theory of irreversible processes. I. General theory and simple applications to magnetic and conduction problems", J. Phys. Soc. Jpn **12**, 570–586 (1957).

[36] M. E. Tuckerman, *Statistical mechanics: theory and molecular simulation* (Oxford university press, 2010).

[37] G. Guennebaud, B. Jacob, et al., *Eigen v3*, 2010.

[38] F. Donado, R. E. Moctezuma, L. López-Flores, M. Medina-Noyola, and J. L. Arauz-Lara, "Brownian motion in non-equilibrium systems and the Ornstein-Uhlenbeck stochastic process", Sci. Rep. **7**, 12614 (2017).

[39] Y. Yan, Y. Liu, T. Xing, and Q. Shi, "Theoretical study of excitation energy transfer and nonlinear spectroscopy of photosynthetic light-harvesting complexes using the nonperturbative reduced dynamics method", Wiley Interdiscip. Rev. Comput. Mol. Sci. **11**, `10.1002/wcms.1498` (2021).